

A millisecond micromixer *via* single-bubble-based acoustic streaming†

Daniel Ahmed,^a Xiaole Mao,^{ab} Jinjie Shi,^a Bala Krishna Juluri^a and Tony Jun Huang^{*ab}

Received 24th February 2009, Accepted 28th May 2009

First published as an Advance Article on the web 23rd June 2009

DOI: 10.1039/b903687c

We present ultra-fast homogeneous mixing inside a microfluidic channel *via* single-bubble-based acoustic streaming. The device operates by trapping an air bubble within a “horse-shoe” structure located between two laminar flows inside a microchannel. Acoustic waves excite the trapped air bubble at its resonance frequency, resulting in acoustic streaming, which disrupts the laminar flows and triggers the two fluids to mix. Due to this technique’s simple design, excellent mixing performance, and fast mixing speed (a few milliseconds), our single-bubble-based acoustic micromixer may prove useful for many biochemical studies and applications.

Introduction

Rapid mixing and homogenization of chemical/biological species on the microscale is of great importance for a wide variety of applications, including chemical kinetics studies¹ and nano-material synthesis.² To probe the transient events which occur during rapid chemical/biological processes or to achieve optimum synthesizing results, reactants have to be mixed within a short period of time (a few milliseconds or less) before the reaction can proceed. Due to the low Reynolds number of most microfluidic devices, this is difficult to achieve.^{3–5} Thus far, droplet-based chaotic advection^{6,7} and hydrodynamic focusing^{1,8,9} have proven to mix fluids within the millisecond range; however, in droplet-based micromixers, a foreign organic phase, which could cause contamination, has to be introduced into the reactants to generate droplets. On the other hand, micromixers based on hydrodynamic focusing^{8–12} may achieve rapid mixing in the focused central stream, but the technique is not applicable across the entire channel’s cross-section.

To overcome the limitations associated with droplet-based and hydrodynamic focusing-based mixing methods, researchers are developing techniques that actively agitate the fluids to achieve mixing.^{13–22} Among these techniques, acoustic-based mixers have attracted a great deal of attention due to their non-invasive²³ nature and simple mixing mechanism. In these mixers, ultrasonic waves, generated by acoustic transducers, propagate inside the fluid media, inducing pressure waves that disturb flow and result in improved mixing efficiency.^{24–30}

Recently, it has been shown that when microbubbles are present in fluid media, mixing efficiency can be further improved. The improved mixing efficiency is due to the acoustic streaming phenomenon,³¹ which “focuses” acoustic energy on an oscillating bubble membrane, resulting in more prominent perturbation to the surrounding fluids. Therefore, bubble-based acoustic

mixers^{32,33} can potentially provide a simple and cost-effective solution to the barriers of current fast micromixing techniques. In this article, we demonstrate a single-bubble-based acoustic mixer that achieves mixing and homogenization of side-by-side laminar microflows within a few milliseconds. To the best of our knowledge, this device presents the fastest mixing speed among currently reported acoustic-based mixers.

Device operation mechanism

The design of our single-bubble-based mixer features a “horse-shoe” shaped microstructure fabricated inside a microfluidic channel (Fig. 1). When the channel is filled with to-be-mixed solutions, the liquids pass by the horse-shoe structure and induce a single bubble due to surface tension³² (see Video 1 in ESI for the bubble trapping process†). The design of the horse-shoe structure ensures that the bubble can be securely trapped inside the microchannel even at high flow rates. It also enables the bubble to perturb the laminar flow exactly at the interface of the two chemical species with maximized efficiency.

When driven by an adjacent acoustic transducer, the membrane of the trapped bubble begins to oscillate. Oscillations generate fluctuations in the velocity and pressure of the

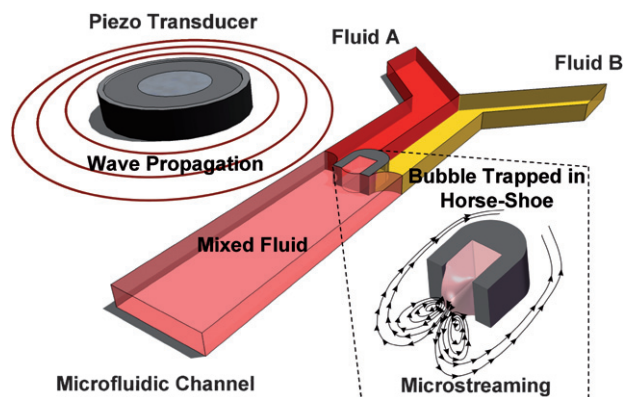


Fig. 1 Schematic of experimental setup. The piezo transducer is placed adjacent to the microfluidic device. Inset: illustration of a bubble trapped inside the horse-shoe structure and streaming pattern around the bubble membrane in the presence of acoustic waves.

^aDepartment of Engineering Science and Mechanics, The Pennsylvania State University, University Park, PA, 16802, USA. E-mail: junhuang@psu.edu; Fax: +814-865-9974; Tel: +814-863-4209

^bDepartment of Bioengineering, The Pennsylvania State University, University Park, PA, 16802, USA

† Electronic supplementary information (ESI) available: Device fabrication and calculation details, and videos for Fig. 1 to Fig. 3. See DOI: 10.1039/b903687c

surrounding fluid, resulting in a strong recirculating flow pattern throughout the liquid near the bubble. This phenomenon is known as acoustic streaming³¹ and is most efficient when the bubble is excited at its resonance frequency. The resonance frequency, f , of an acoustically driven bubble can be estimated by the small-amplitude behavior of the Rayleigh–Plesset equation,³⁴

$$f^2 = \frac{1}{4\rho\pi^2 a^2} \left\{ 3\kappa \left(p + \frac{2\sigma}{a} \right) - \frac{2\sigma}{a} \right\} \quad (1)$$

where ρ is the density of the liquid (kg m^{-3}), σ is the surface tension of solution (N m^{-1}), k is the polytropic exponent for a bubble containing air, p is the fluidic pressure (N m^{-1}), and a is the radius of the bubble (m).

Experimental details

A polydimethylsiloxane (PDMS) based microchannel was fabricated using standard soft lithography and mold replica technique. Its width, depth, and length were $240 \mu\text{m}$, $155 \mu\text{m}$, and 1 cm , respectively. The horse-shoe structure was positioned at the center of the channel. The width, length and height of the horse-shoe trap were 60 , 90 and $155 \mu\text{m}$, respectively. The PDMS channel was activated using oxygen plasma and bonded to a plastic petri-dish. A piezo transducer (Model No. 273-073, Radioshack) was bonded adjacent to the PDMS microfluidic device on the same plastic substrate using epoxy. Experimentally, we observed that acoustic streaming was more prominent on plastic substrates than on glass substrates. This phenomenon is attributed to the low acoustic impedance mismatch between epoxy and plastic substrates. The piezo transducer was driven by a function generator (Hewlett Packard 8116A) at a frequency and voltage of 70.1 kHz and 8 V (peak to peak), respectively. Experimentally, the resonance frequency was determined by sweeping the excitation frequency with a 100 Hz increment near the theoretically calculated resonance frequency. At the resonance frequency, the acoustic streaming near the bubble surface was prominent, reflecting maximum bubble oscillation.

Results and discussions

Fig. 2 shows the characterization of the fluidic flow pattern near an acoustically excited microbubble trapped in a horse-shoe structure. A solution of polystyrene particles (diameter = $1.9 \mu\text{m}$, in DI water) was first injected into the channel using a syringe pump (KD Scientific-210), and a single air bubble was trapped within the horse-shoe structure due to the liquid/air interface and the hydrophobic–hydrophilic interaction between the PDMS horse-shoe structure and the fluid.³² Experimentally, we observed that the size and shape of the bubble trapped within the structure is repeatable and it is unnecessary to pretreat the channel. From the image of the air bubble membrane (Fig. 2a), we estimated the radius of the bubble to be around $41 \mu\text{m}$. The resonance frequency of the trapped bubble can then be calculated to be 81.6 kHz using eqn (1) (detailed calculation is available in the ESI†). Experimentally, the resonance frequency was measured to be 70.1 kHz . The discrepancy between the experimental and theoretical resonance frequencies can be attributed to the oblate shape of the air bubbles in the experiments since a spherical shape was assumed for theoretical calculation.

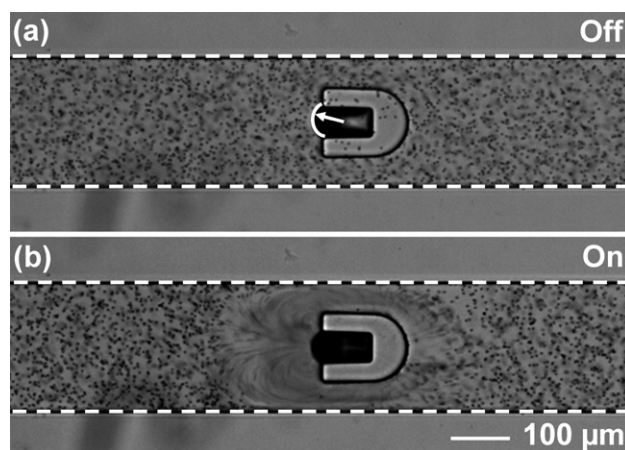


Fig. 2 Characterization of the acoustic streaming pattern around a single bubble. (a) An air bubble trapped in the horse-shoe structure and stationary polystyrene particle solution. (b) Recirculating flow pattern around the air bubble when the bubble membrane oscillates at its resonance frequency.

Fig. 2a shows that the particle flow was nearly stationary prior to the acoustic agitation. As the membrane of the air bubble was excited by the piezo transducer, acoustic streaming was induced in the liquid near the bubble interface. The acoustic streaming phenomenon is made visible in Fig. 2b through the trajectories of the polystyrene particles. The streaming pattern was characterized by a pair of counter-rotating vortices (double-ring recirculation flows), which originated from the bubble's membrane and extended from the frontside to the backside of the horse-shoe structure. These double-ring recirculation flows caused by acoustic streaming were located in the upper and lower half of the channel, respectively. The recirculation flow significantly enhanced the mass transport efficiency in the laminar flow^{5,6,35} and resulted in rapid mixing. A video showing the microstreaming phenomenon can be found in the ESI (Video 2 in ESI).†

To characterize the mixing performance of our single-bubble-based mixer, DI water and fluorescent dye (fluorescein) were injected into the channel from each inlet at flow rates of $8 \mu\text{l/min}$. Fig. 3a shows the side-by-side laminar flow before and after passing by the horse-shoe structure when the bubble was at rest. No significant mixing was observed due to the absence of acoustic perturbation. The trapped air bubble was subsequently excited at its resonance frequency. Acoustic streaming due to the bubble membrane oscillations perturbed the fluidic interface. The strong vortical fluidic flow facilitated the rapid interchanging of liquid between the two streams, enabling fast and homogenized mixing (Fig. 3b). A video showing the same mixing process can be found in the ESI (Video 3 in ESI).†

The mixing performance was evaluated by measuring the gray-scale value of the images obtained, a good indicator for the fluorescent dye concentration. The cross-sectional dye concentration profile after bubble-induced acoustic streaming (the vertical dashed line in Fig. 3b) were measured and normalized against its own peak intensity (Fig. 3c). The intensity profile indicates that after the acoustic streaming took place, a uniform gray-scale distribution across the width of channel was observed, suggesting excellent mixing of the two chemical species.

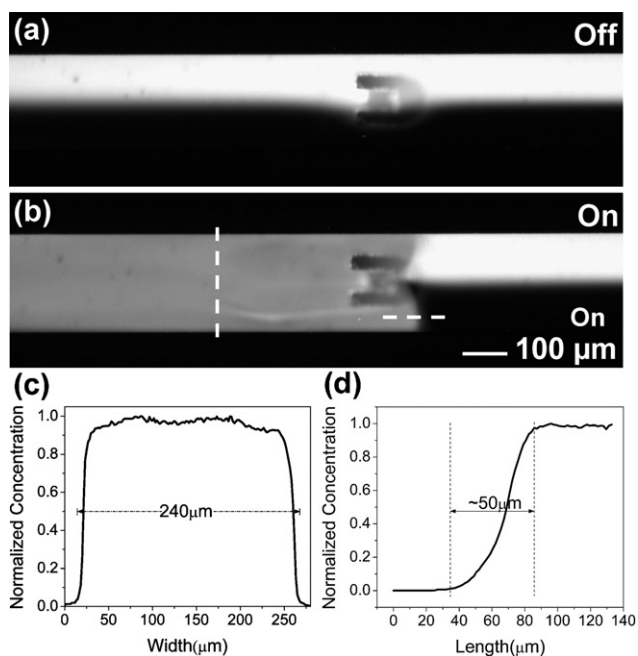


Fig. 3 Characterization of the mixing efficiency. (a) No mixing effect was observed in absence of acoustic waves. (b) Homogenized mixing of DI water and fluorescent dye in presence of acoustic waves. (c) Plot of normalized fluorescent concentration across the channel width. (d) Plot of normalized fluorescent concentration along the channel length from unmixed to mixed regions near the horse-shoe structure.

We further characterized the mixing time of the mixer. The average mixing time (t) was estimated using the equation,

$$t = d_{mix}/v_{avg} \quad (2)$$

where t is the mixing time, d_{mix} is the distance from unmixed to completely mixed regions, and v_{avg} is the average fluid velocity. In order to estimate d_{mix} in Fig. 3b, we plotted the normalized gray-scale values along the length of the channel from the unmixed to mixed region (the horizontal dashed line in Fig. 3b). From the plot, d_{mix} was measured to be approximately 50 μm . v_{avg} was determined to be 7.2 mm s^{-1} by dividing the combined flow rate (16 $\mu\text{l min}^{-1}$) by the cross-sectional area of the channel. The mixing time was therefore determined to be ~ 7 ms, which is significantly faster than response times reported for existing acoustic-based micromixers (mixing time: seconds to tens of seconds).^{24,26–29}

One concern is that the curvature of the bubble trapped in the horse-shoe structure may be changed upon different flow rates. To date, there are no theoretical models that can precisely estimate the natural frequency of bubbles with different shapes. To compensate for the change in the curvature of bubbles at different flow rates, the excited frequency should be experimentally adjusted (by sweeping the excitation frequency with small increments near the predicted frequency). Experimentally we observed that as we changed the flow rate from 3 $\mu\text{l/min}$ to 10 $\mu\text{l/min}$, the natural frequency of the bubble changed less than 5%. For such a small shift in natural frequency, the mixing performance remained unaltered. Another factor that could affect the mixing performance is surface tension. Future research will be directed to

applying this mixing technique to real biological and chemical applications, in which a variety of soluble compounds, biomolecules, and chemicals are involved. In these applications, the effects of surface tension will need to be thoroughly investigated.

In conclusion, we have demonstrated a prototype active microfluidic mixer based on the acoustic streaming phenomenon around a single air bubble trapped by a horse-shoe structure inside a microchannel. The vibration of the air bubble at its resonance frequency allows the perturbation of the fluidic interface, which significantly improves the mixing performance. Through quantitative analysis, we have proven that our mixer can achieve excellent homogenized mixing across the entire width of the channel with a mixing time of ~ 7 ms. With optimization of device geometry, flow condition and the implementation of the acoustic-energy-focusing components,^{36,37} the mixing time could be further reduced to the sub-millisecond regime. We believe that based on the device's simple design, excellent homogenization, and fast mixing speed, our single-bubble-based acoustic mixer will benefit a variety of on-chip biological and chemical studies and applications.

Acknowledgements

We thank Sz-Chin Steven Lin, Padma Kumar, Jaya Prakash Koduru, Sahar Louyeh and Aitan Lawit for helpful discussion. This research was supported by National Science Foundation (ECCS-0824183 and ECCS-0801922) and the Penn State Center for Nanoscale Science (MRSEC). Components of this work were conducted at the Penn State node of the NSF-funded National Nanotechnology Infrastructure Network.

References

- 1 L. Pollack, M. W. Tate, N. C. Darnton, J. B. Knight, S. M. Gruner, W. A. Eaton and R. H. Austin, *Proc. Natl. Acad. Sci. U.S. A.*, 1999, **96**, 10115.
- 2 J. deMello and A. deMello, *Lab Chip*, 2004, **4**, 11N–15N.
- 3 C. M. Ho and Y. C. Tai, *J. Fluids Eng.*, 1996, **118**, 437.
- 4 G. M. Whitesides, *Nature*, 2006, **442**, 368–373.
- 5 X. Mao, J. R. Waldeisen and B. K. Juluri, *Lab Chip*, 2007, **7**, 1303–1308.
- 6 H. Song and R. F. Ismagilov, *J. Am. Chem. Soc.*, 2003, **125**, 14613.
- 7 E. M. Miller and A. R. Wheeler, *Anal. Bioanal. Chem.*, 2009, **393**, 419–426.
- 8 J. B. Knight, A. Vishwanath, J. P. Brody and R. H. Austin, *Phys. Rev. Lett.*, 1998, **80**, 3863–3866.
- 9 H. Y. Park, X. Qiu, E. Rhoades, J. Korlach, L. W. Kwok, W. R. Zipfel, W. W. Webb and Lois Pollack, *Anal. Chem.*, 2006, **78**(13), 4465–4473.
- 10 T. H. Wang, Y. Peng, C. Zhang, P. K. Wong and C. M. Ho, *J. Am. Chem. Soc.*, 2005, **127**, 5354–5359.
- 11 X. Mao, J. R. Waldeisen and T. J. Huang, *Lab Chip*, 2007, **7**, 1260–1262.
- 12 X. Mao, S. S. Lin, C. Dong and T. J. Huang, *Lab Chip*, 2009, **9**, 1583–1589.
- 13 H. Chun, H. C. Kim and T. D. Chung, *Lab Chip*, 2008, **8**, 764–771.
- 14 H.-P. Chou, M. A. Unger and S. R. Quake, *Biomed. Microdevices*, 2001, **3**, 323.
- 15 C. K. Harnett, J. Templeton, K. A. Dunphy-Guzman, Y. M. Senousy and M. P. Kanouff, *Lab Chip*, 2008, **8**, 565–572.
- 16 M. Sigurdson, D. Wang and C. D. Meinhart, *Lab Chip*, 2005, **5**, 1366–1373.
- 17 L. Johansson, S. Johansson, F. Nikolajeff and S. Thorslund, *Lab Chip*, 2009, **9**, 297–304.
- 18 K. S. Ryu, K. Shaikh, E. Goluch, Z. Fan and C. Liu, *Lab Chip*, 2004, **4**, 608–613.

-
- 19 A. N. Hellman, K. R. Rau, H. H. Yoon, S. Bae, J. F. Palmer, K. S. Phillips, N. L. Allbritton and V. Venugopalan, *Anal. Chem.*, 2007, **79**, 4484–4492.
- 20 W. Y. Ng, S. Goh, Y. C. Lam, C. Yang and I. Rodriguez, *Lab Chip*, 2009, DOI: 10.1039/b813639d.
- 21 L. Gui and C. L. Ren, *Anal. Chem.*, 2006, **78**, 6215–6222.
- 22 J. T. Coleman, J. McKechnie and D. Sinton, *Lab Chip*, 2006, **6**, 1033–1039.
- 23 J. Shi, X. Mao, D. Ahmed, A. Colletti and T. J. Huang, *Lab Chip*, 2008, **8**, 221–223.
- 24 G. G. Yaralioglu, I. O. Wygant, T. C. Marentis and B. T. Khuri-Yakub, *Anal. Chem.*, 2004, **76**, 3694–3698.
- 25 K. Sritharan, C. J. Strobl, M. F. Schneider, A. Wixforth and Z. Guttenberg, *App. Phys. Lett.*, 2006, **88**, 054102.
- 26 T. Frommelt, M. Kostur, M. Wenzel-Schafer, P. Talkner, P. Hanggi and A. Wixforth, *Phys. Rev. Lett.*, 2008, **100**, 034502.
- 27 A. Wixforth, C. Strobl, C. Gauer, A. Toegl, J. Scriba and Z. V. Guttenberg, *Anal. Bioanal. Chem.*, 2004, **379**, 982–991.
- 28 Z. Yang, S. Matsumoto, H. Goto, M. Matsumoto and R. Maeda, *Sens. Actuators, A*, 2001, **93**, 266–272.
- 29 W. K. Tseng, J. L. Lin, W. C. Sung, S. H. Chen and G. B. Lee, *J. Micromech. Microeng.*, 2006, **16**, 539–548.
- 30 H. Yu, J. W. Kwon and E. S. Kim, *J. Microelectromech. Syst.*, 2006, **15**(4), 1015–1024.
- 31 P. Marmottant and S. Hilgenfeldt, *Nature*, 2003, **423**, 153–156.
- 32 A. R. Tovar and A. P. Lee, *Lab Chip*, 2009, **9**, 41–43.
- 33 R. H. Liu, J. Yang, M. Z. Pindera, M. Athavale and P. Grodzinski, *Lab Chip*, 2002, **2**, 151–157.
- 34 T. G. Leighton, *The Acoustic Bubble*, Academic Press, London, 1994.
- 35 X. Mao, S. S. Lin, M. I. Lapsley, J. Shi, B. K. Juluri and T. J. Huang, *Lab Chip*, 2009, DOI: 10.1039/B822982A.
- 36 J. Shi, S. S. Lin and T. J. Huang, *App. Phys. Lett.*, 2008, **92**(11), 111901.
- 37 S. S. Lin, T. J. Huang, J. Sun and T. T. Wu, *Phys. Rev. B*, 2009, **79**, 094302.